PROCEEDINGS, 50th Workshop on Geothermal Reservoir Engineering
Stanford University, Stanford, California, February 10-12, 2025
SGP-TR-229

Coupled Numerical and Analytical Simulation on the Delft Campus Geothermal Well

Yuan Chen[1], Guillaume Rongier[1], James Robert Mullins[2], Denis Voskov[1,3] and Alexandros Daniilidis[1]

[1]Department of Geoscience & Engineering, TU Delft, Stevinweg 1, 2628 CN Delft, Netherlands

[2]Department of Energy Science & Engineering, Stanford University, Stanford, CA 94305, USA

[3]Rock Flow Dynamics, Berliner Freiheit 3, 28327, Bremen, Germany

y.chen-21@tudelft.nl

Keywords: geothermal doublet, direct-use heating uncertainty quantification, numerical simulation, analytical solution, water loss

ABSTRACT

With the growing interest in geothermal energy as a green, local solution to mitigate green house gas (GHG) emission, accurate representation of geological uncertainty is critical. The Delft campus geothermal project aims to provide clean heating for the campus buildings and surrounding parts of the city. In this work, we evaluate the thermal response of the geothermal system under a range of potential subsurface uncertainties using coupled numerical and analytical methods. An initial ensemble of geological models using data collected during the drilling campaign combined with regional studies was generated to capture the wide range of geological uncertainty. We perform a static analysis on the heterogeneity level of all geological models. Subsequently, the geological models are dynamically simulated in the open-source software Delft Advanced Research Terra Simulator (open-DARTS). In this work, we find the introduction of GTD (Geothermie Delft) data reduce the uncertainty range. We also demonstrate that there can be a significant variation in our assessment of the lifetime of the geothermal system and the extent of the cold plume front with subtle variations in subsurface heterogeneity. Additionally, our study reveals that all 120 geological models exhibit injection well BHP values below the government (SodM) regulations. Furthermore, there is a potential hydraulic connection between the reservoir layers and the layers above the reservoir due to the loss of an initial borehole that is now abandoned. We design a coupled analytical radial flow and numerical simulation framework to estimate the risk of water losses and the cold front propagation within the layers above the target reservoir. We find that the geological uncertainties, especially the permeability and thickness, prominently affect the prediction of water losses. the result shows that 1.5% to 20% of the original discharge rate flows to the upper layers.

1. INTRODUCTION

Geothermal energy has been developed and exploited for a long time to generate electricity or to apply in non-electrical uses such as greenhouse and direct heating (Lund & Toth, 2021). The low-enthalpy direct-use geothermal project on the campus of the Delft University of Technology (with the name “Geothermie Delft”) has been initiated to provide a unique research environment, alongside commercial thermal energy production for heating TU Delft’s campus and parts of the city of Delft (Bruhn et al., 2015; Vardon et al., 2024). A geothermal doublet has been successfully installed on TU Delft campus during the second half of 2023, with initial energy production planned for 2025.

During the drilling campaign, well-log data, core data, and well-test data have been extensively collected (Barnhoorn et al., 2024). Despite these extensive data collection initiatives, the inherent complexity of geological uncertainty and limited spatial data away from the wells necessitate computer models to gain comprehensive reservoir scale understanding. Geological modeling is essential for geothermal production to predict resource distribution and exploitation potential (Babaei & Nick, 2019). It is also the basis for informed optimization and decision-making in field operations. However, there is limited published work incorporating the Delft campus geothermal well data to create a representative field-scale geological model. Voskov, Abels, et al. (2024) created an ensemble of geological models using existing subsurface data in the West Netherlands Basin that shows that the uncertainty in geological characterization results in a large spread of the production temperature and well BHP.

Reservoir heterogeneity is considered as the degree of variation of reservoir properties, e.g. permeability and porosity anisotropy at different scales (Tiab & Donaldson, 2016). Two coefficients, the Lorenz coefficient and the Dykstra-Parsons permeability variation, are used to describe the level of macroscopic heterogeneity in reservoirs (Tiab & Donaldson, 2016). Reservoir heterogeneity in hydraulic properties such as porosity has a large impact on the geothermal reservoir performance (Liu et al., 2019; Major et al., 2023). The heterogeneity of the geological system can significantly affect the thermal response of a geothermal project.

Based on the geological models, numerical simulation is employed to assess the feasibility and risk at essential phases of projects. It provides a long-term and reservoir-scale understanding of the fluid flow in porous media and the interaction of the injected fluid with rock and in-situ fluid (Pandey et al., 2018). In addition to numerical simulation, analytical solutions can provide a computationally efficient and accurate result without setting up a mesh and boundary conditions, and have been proven to work well for simplified, homogeneous models (Carslaw &Jaeger, 1959; Muskat, 1936).

In this work, we first describe the detailed workflow to create multiple high-fidelity geological models based on the GTD well data. We then present the evaluation of the heterogeneity level for all the models. Meanwhile, we use the same structural model, however, the GTD

data is removed to do the facies modeling. Subsequently, we utilize these high-fidelity geological models to perform the dynamic thermal production simulation to investigate the effect of the heterogeneity on production temperature, wells' BHP and the cold plume extent propagation. In the end, we apply a coupled numerical and analytical approach to investigating the effect of the abandoned wellbore, assumed to be open and hydraulically connected, on the cold front propagation inside the upper layers.

2. DATA AND METHODS

An ensemble of facies realizations that honor the geological data from the Delft campus geothermal doublet has been generated. We statically and dynamically analyze these geological realizations. Firstly, we create the facies models based on the lithofacies determined by the shale volume cutoff using object-based channel simulation. Secondly, we populate the porosity for different lithofacies using the Sequential Gaussian Simulation (SGS) approach. Subsequently, we distribute permeability using the porosity-permeability relationship derived from Willems et al.(2020). We investigate the heterogeneity level of all geological models using the Lorenz coefficient (LC) and the coefficient of variation namely the Dijkstra-Parsons (DP) coefficient. Next, we perform dynamic simulations to investigate how the thermal response is affected by geological heterogeneity. Finally, we apply a coupled numerical and analytical approach to investigate the effect of the abandoned borehole on Delft campus geothermal production

2.1 Geological data

We use subsurface data (TNO, 1977) from the Nieuwerkerk Formation in the Western Netherlands Basin (WNB) to constrain geological models representing a wide range of heterogeneity. This study specifically leverages data from the Delft campus geothermal wells (Barnhoorn et al., 2024) to examine the impact of reservoir heterogeneity on thermal production. The target aquifer layer is the Delft sandstone member which conformably overlies the Alblasserdam member and has been interpreted as meandering river deposits (Donselaar & Overeem, 2008). The seismic data and well logs suggest a reservoir thickness of ca. 120 m. We mainly use gamma-ray (GR) logs to compute shale volume at the depth indicated in Figure 1, because GR data is the only data present for all wells in the study area. We apply the Stieber model (Stieber, 1970) to estimate the shale volume based on GR data based on the following two equations eqs. (1) and (2):

$$I_{\mathrm{GR}} = \frac{GR_{\log} - GR_{min}}{GR_{max} - GR_{min}} \tag{1}$$

$$V_{\mathrm{sh}} = \frac{I_{\mathrm{GR}}}{3 - 2 \cdot I_{\mathrm{GR}}} \tag{2}$$

where, I_{GR} [-] is the relative amplitude of the GR intensity, GR_{log} [API unit] is the gamma ray log values, GR_{min} [API unit] and GR_{max} [API unit] are the minimum and maximum gamma ray values respectively, V_{sh} [-] is the shale volume ratio. Figure 1shows the shale volume ratio of 10 wells within the study area. DEL-GT-01 and DEL-GT-02-S2 are the GTD production and injection wells respectively.

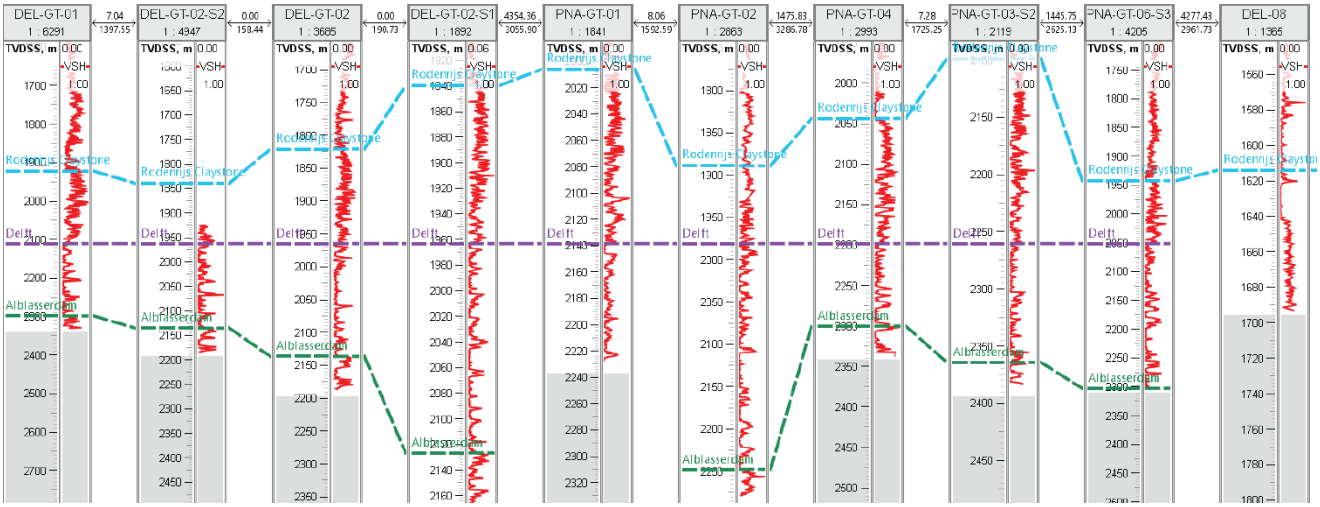

Figure 1: The shale volume calculated based on Gamma-ray (GR) logs from 10 wells including the Delft campus geothermal doublet located in the Western Netherlands Basin (WNB).

We define the discrete lithofacies log based on the shale volume ratio cut-off (Dejtrakulwong et al., 2009). Three ranges of shale volume ratio values identify three lithofacies: coarse sand, fine sand and shale (Table 1). This initial lithofacies log well data including the data from the GTD wells is then blocked to the grid resolution using the most frequent facies in each block. We use these blocked lithofacies to constrain the static facies models. We fit the variogram using the blocked lithofacies log data within the research area. Table 2 and Table 3 summarize the fitted variogram parameters describing the spatial continuity of each lithofacies within the Delft sandstone member.

We also fitted porosity using the Sequential Gaussian Simulation (SGS) method, but not in facies modeling. Thus, we minimize the risk of bias caused by the poor variogram fitting resulting from the limited amount of upscaled porosity data from the available wells.

Table 1. Shale volume ration based on facies distribution

Range	Lithofacies
$V_{sh} \leq 0.2$	Coarse sand
$0.2 < V_{sh} < 0.3$	Fine sand
$V_{sh} \geq 0.3$	Shale

Table 2. Fitted variogram parameters (with GTD wells data)

Lithofacies	Major direction range (m)	Minor direction range (m)	Vertical direction range (m)	Azimuth (°)	Sill
Shale	427.43	342.58	3.33	251.11	0.19
Fine sand	1124.64	951.62	3.31	327.89	0.19
Coarse sand	345.33	312.89	6.31	277.87	0.24

Table 3. Fitter variogram parameters (without GTD wells data)

Lithofacies	Major direction range (m)	Minor direction range (m)	Vertical direction range (m)	Azimuth (°)	Sill
Shale	1177.28	1066.38	8.86	267.57	0.097
Fine sand	576.18	468.15	3.33	348.66	0.22
Coarse sand	674.17	656.88	3.33	337.94	0.25

2.2 Geological static modelling

We first create a basin-scale structural model incorporating the geological data from the wells located in the Western Netherlands Basin (WNB). Then we apply Object-based (OBS) to simulate the facies distribution. OBS is a commonly used facies modeling approach that uses geometric shapes e.g., channels, lobes to represent depositional features as discrete objects in the model (Holden et al., 1998). These objects are stochastically distributed based on geological rules, such as depositional environments and dimensions derived from analogs or well data. Table 4 gives the parameters of OBS. The geological model process is fully performed in Rock Flow Dynamics (2024).

Table 4. Channel properties and target proportions

Parameters	Min Value	Mode Value	Max Value
Channels Width (m)	30	50-300	600
Levee Width Fraction	0.5	1.5	2.0
Channels Thickness (Gilding, 2010) (m)	1.5	3.0	4.5
Levee Thickness Fraction	0.5	0.7	0.9
Channels Azimuth (Gilding, 2010) (degrees)	300	315	330
Channels Sinuosity Length (m)	1000	1500	2000
Channels Sinuosity Amplitude (m)	200	500	800
Channels Relative Sinuosity	0.2	0.3	0.4
Net to Gross (N/G)		0.2-0.8	

2.3 Numerical model

Within geothermal reservoir simulation, the governing equations include mass and energy conservation with closure assumptions on the thermal equilibrium between different phases including the solid. Typically, the fully coupled, fully implicit scheme finds application in numerical geothermal simulations due to its unconditional stability. In this study, we use the open-source Delft Advance Research Terra Simulator (open-DARTS) (Voskov, Saifullin, et al.,2024) employing a fully implicit solution with the finite volume method alongside the two-point flux approximation to discretize these governing equations. Conservation equations governing geothermal applications can be written in the following form:

$$\frac{\partial}{\partial t}\left(\phi \sum_{j=1}^{n_p} \rho_j s_j\right) - \nabla \cdot \sum_{j=1}^{n_j} \rho_j v_j + \sum_{j=1}^{n_p} \rho_j \tilde{q_j} = 0, \tag{3}$$

$$\frac{\partial}{\partial t}\left(\phi \sum_{j=1}^{n_p} \rho_j s_j U_j + (1-\phi) U_r\right) - \nabla \cdot \sum_{j=1}^{n_p} h_j \rho_j v_j + \nabla \cdot (\kappa \nabla T) + \sum_{j=1}^{n_p} h_j \rho_j \tilde{q_j} = 0, \tag{4}$$

where t denotes time, ϕ the porosity of the media, n_p the total number of phases existing in the geothermal system, ρ_j the density of phase j, s_j the saturation of phase j, $\tilde{q_j}$ the phase rate per unit volume, U_j the phase internal energy, U_r the internal energy of rock, v_j the Darcy velocity of phase j, h_j the phase enthalpy and T the temperature. Table 5 describes the major parameters used for the models. The initial

distribution of pressure and temperature is following the natural gradient. We designate properties of sandstone and shale in the model based on the 0.1 porosity cutoff. If the porosity is less than 0.1, we assign the property of the shale to the cell, otherwise we assign the property of sandstone. For the numerical setup and grid resolution, we follow the findings as presented in Chen et al., 2025.

2.4 Analytical models

A simplified steady-state radial flow is applied to evaluate the water rate within the layers above the reservoir. The steady-state model is coupled to the reservoir simulation model as described in section 3.1. The relationship between BHP and the water flow rate in the motherbore is:

$$p_r - p_w = \frac{q_{sc} B \mu}{2\pi k h} \ln(r_e / r_w + s) \tag{5}$$

where p_r and p_w are reservoir pressure [Pa] and bottom-hole pressure [Pa] respectively, q_{sc} flow rate at surface conditions [m3/s], B the fluid compressibility [m3/m3], μ fluid viscosity [Pa · s], k matrix permeability [m2], r_e reservoir radius [m], r_w wellbore radius [m] and s skin factor [-]. This analytical formula is written under simplifying assumptions that the permeable reservoir above the target reservoir is infinite and the pressure pr in the reservoir is not changing with time.

Table 5. Parameter settings for reservoir model

Parameters	Value
Original grid dimension	$413 \times 382 \times 200$
Cropped grid dimension	$167 \times 154 \times 200$
Grid size, m	$20 \times 20 \times (0.21 - 2.71)$
Permeability, mD	(0.004–2705)
Porosity, -	(0.01–0.35)
Sandstone heat capacity, kJ/m^3/K	2450
Sandstone heat conductivity, kJ/m/day/K	259.2
Shale heat capacity, kJ/m^3/K	2300
Shale heat conductivity, kJ/m/day/K	190.08
Temperature gradient, K/km	30
Pressure gradient, bars/km	100
Injection temperature, K	298.15
Discharge rate, m^3/day	8400

3. RESULTS

3.1 Geological models

3.1.1 Facies models

We run OBS to generate 120 basin-scale geological facies models. The example 3D facies models from cases constrained by GTD wells and cases without incorporating the GTD wells are shown in Figure 2 with the same structural model. The blue and red tubes indicate the locations and trajectories of the injection well and the production well respectively. A representation of the spatial facies distribution is shown in cross section in Figure 3 and Figure 4. All models are generated using the parameters listed in Table 4.

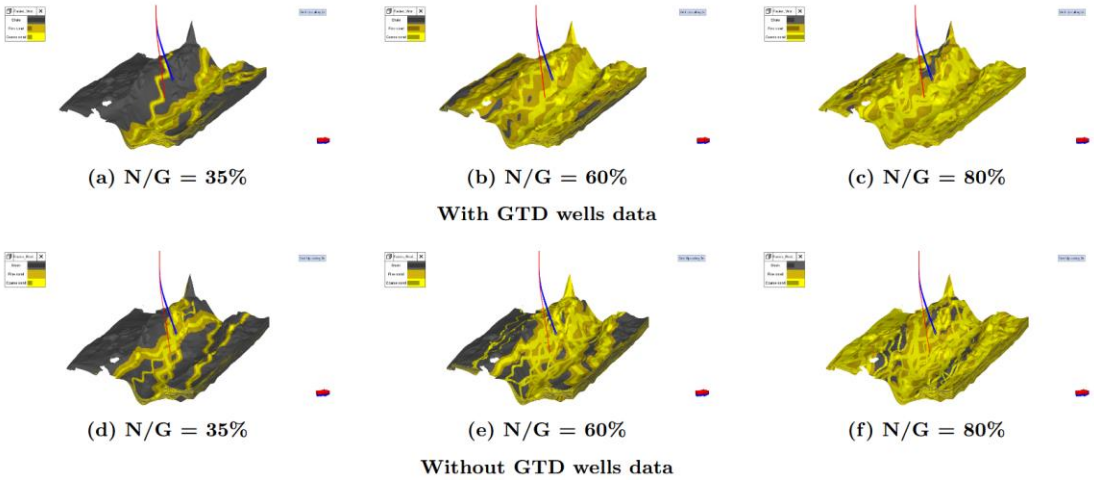

Figure 2. Spatial distribution of facies with different N/G ratio

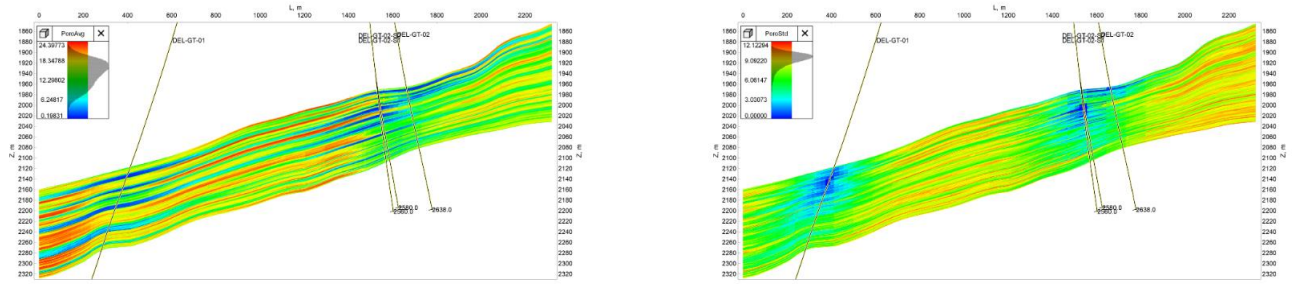

(a) Average porosity (b) Standard deviation porosity

Figure 3. The mean and standard deviation of porosity at the well section for 120 geological models constrained incorporating the GTD wells

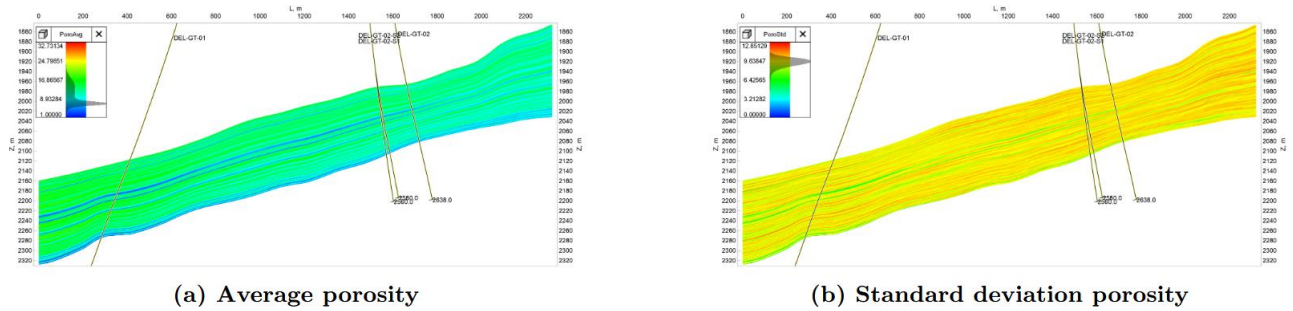

(a) Average porosity (b) Standard deviation porosity

Figure 4. The mean and standard deviation of porosity at the well section for 120 geological models constrained without incorporating the GTD wells

3.1.2 Property models

We then populate the porosity in different lithofacies and evaluate the heterogeneity level of these 120 geological models. Figure 5 shows that the models without GTD wells' data show a larger uncertain range in LC and DP. It means the introduction of the GTD wells' data constrains the geological properties around the designated wells. However, all geological models with or without GTD wells' data are classified as heterogeneous models (Tiab & Donaldson, 2016) according to the LC and DP range.

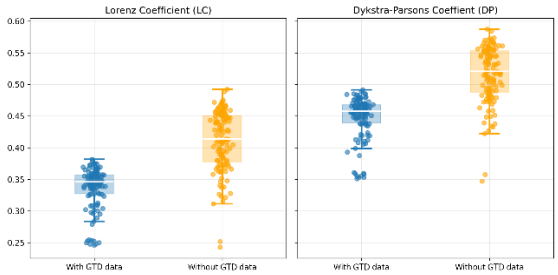

Figure 5. Lorenz coefficient (LC) and Dykstra-Parsons coefficient (DP) of the geological models

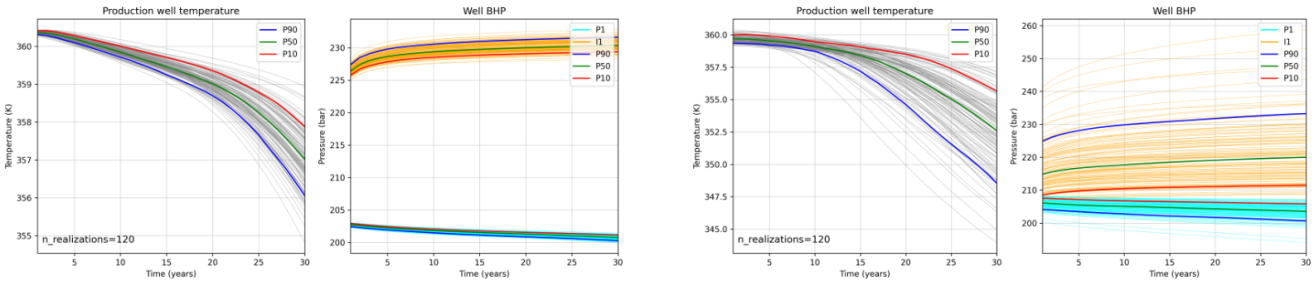

(a) With GTD data (b) Without GTD data

Figure 6. Production temperature and BHP of the doublet

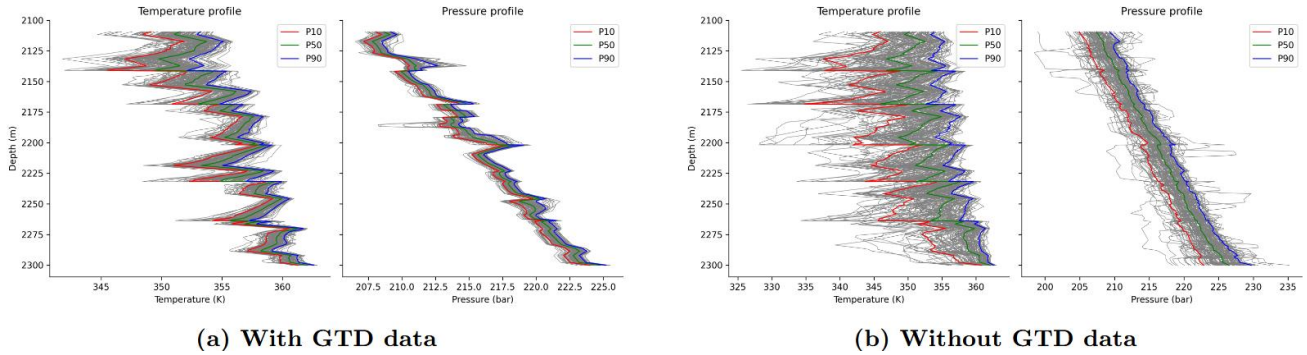

Figure 7. The temperature and pressure profile of the production well at year 30

3.2 Production temperature and Bottom Hole Pressure (BHP)

We plot the temperature and pressure profile for the wells (Figure 6) and along the depth at the production wells of 120 realizations (Figure 7). The temperature profiles along depth for all realizations constrained by GTD wells data exhibit a maximum difference of 15 K, compared to a maximum difference of 25 K in the models not constrained by GTD wells data. Similarly, the pressure profiles along depth from the constrained models show an average difference of 2 bar, whereas the unconstrained models exhibit a larger average difference of 10 bar. The uncertain range of temperature and pressure along depth at the production well shows a strong heterogeneity at that location and can be reduced with the addition of hard constraints from the well data.

3.3 Cold plume extent

Besides the production well temperature and wells' BHP, we also evaluate the cold plume extent for all realizations. We assess the vertical share of the injection temperature of 120 realizations with 200 reservoir layers. The blue dot and red dots show the injection well and production well in the middle of the reservoir. The vertical share of the models without GTD well data is more spread out, indicating that the fluid flow pattern of realizations without GTD well data is more uncertain compared to the realizations constraint by the GTD well data (Figure 8).

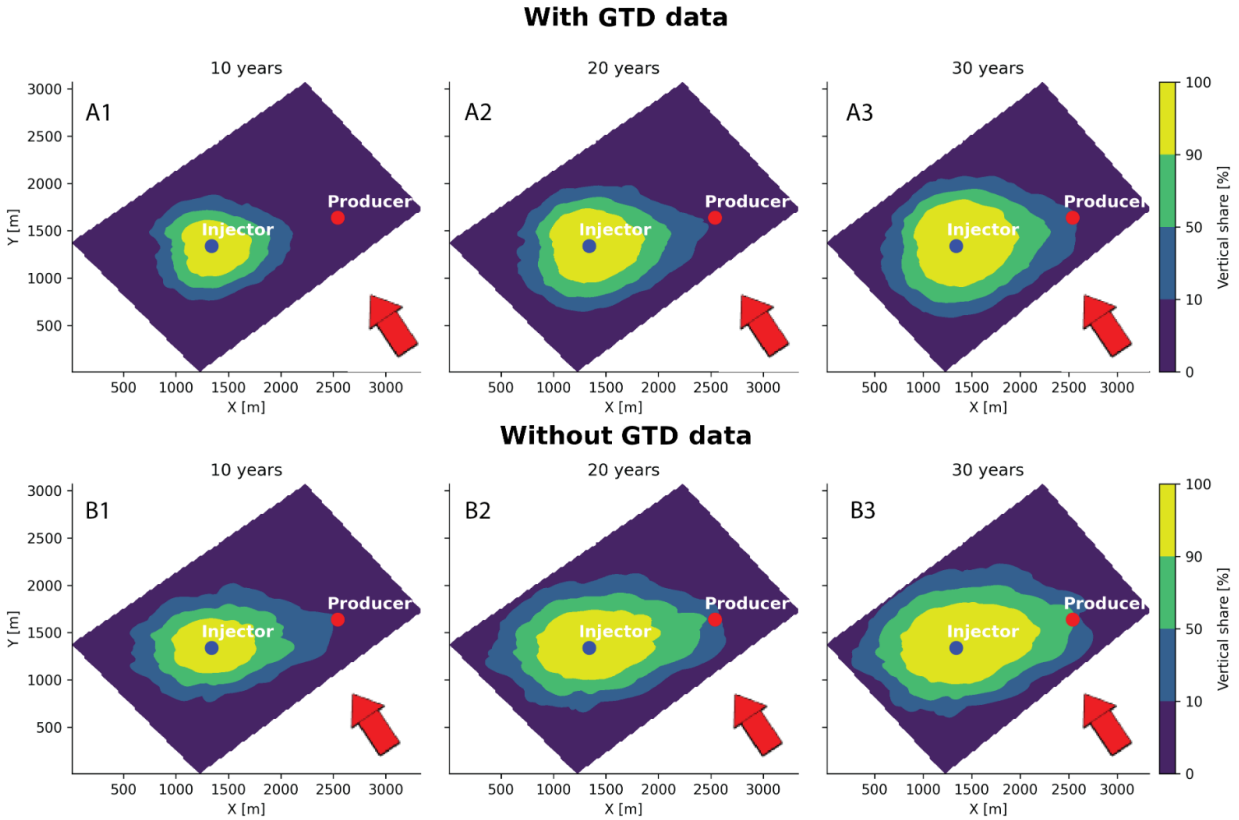

Figure 8. Vertical share of injection temperature at xy plan for the cases with (A1-A3) and without (B1-B3) GTD wells data for different thermal production time (10,20 and 30 years).

3.4 Analytical solution in the upper layers

Due to drilling challenges, the original injection well was lost due to instability, and the abandoned borehole was cemented at 1300 m True Vertical Depth (TVD) only. Below this depth, the lost wellbore remains, possibly as an open hole section called 'motherbore' in the discussion below. The formations Rijswijk sandstone member and Berkel sandstone member can be potentially connected hydraulically to the reservoir. The thickness of these formations, indicated in Figure 9, is interpreted from ThermoGIS (2023) and Willems et al. (2020). A side-track injection well is drilled ca. 100 m from the initial bore. We investigate how much water could be lost to the layers above the reservoir section via the open-hole motherbore due to the elevated pressure following injection from the sidetrack as a worst case scenario. \Cref{fig:schematicview} is a schematic cross-section showing the configuration of the reservoir, the layers above the reservoir, and the wells. Operationally, there are a number of features which are likely to limit this flowrate, some of which are driven by the 2 year period between the drilling and the system operation. The motherbore was filled with an oil-based drilling fluid with a density higher than that of the reservoir fluid. This is calculated to create an overpressure of >14 bar initially, which is likely to be higher than the injection pressure. If the fluid flows into the formations over times, this will create a skin to reduce flow, but also reduce this overpressure. The motherbore is also uncased, and claystones with a similar geological history in the same area have been shown to be unstable. Therefore, is also considered feasible that the Rodenrijs claystone will collapse and/or close reducing the flow.

In this work, we assume that Rodenrijs claystone remains open which is considered the worst case scenario. With this assumption, we incorporate the numerical model with analytical model.. Figure 9 is a schematic cross-section showing the configuration of the reservoir, the layers above the reservoir, and the wells. Here, we used a simplified model for water losses into the upper layers following assumptions on the radial inflow in the infinite reservoir

$$Q_{in} = \frac{2\pi kh}{\mu ln(r_e/r_w+s)}(p_r - p_w) = PI\frac{1}{\mu}(p_r - p_w) \tag{6}$$

where p_r and pw are reservoir pressure and motherbore pressure respectively, Q_{in} is flow loses rate, μ is fluid viscosity, k_h is permeability times thickness of the reservoir layer, r_w is the wellbore radius and s is skin factor and PI is production index. This model is fully coupled with dynamic simulation allowing us to estimate the effect of these losses on the dynamic of production reservoir. The properties used for the upper layers are listed in Table 6.

In this study, we continue the investigation started in Voskov, Abels, et al., 2024 where we constrained an existing geological ensemble of models to the log at the production well, selected a limited number of realizations (18) weakly satisfying these logs, and evaluated water loss to the upper formations based on simplified assumptions. Here we use the full ensemble constrained to the log information for both wells in the process of geological modeling. We assume that the shape and properties of the open-hole section in the motherbore have limited change over time, which is a worst-case scenario. We define the kh, layer thickness and skin factor to generate min and max production index for the losses to the upper layers.

Figure 10 shows the water loss to the upper layers using the coupled numerical and analytical approach. It shows that 1.5% to 20% of the original discharge rate goes to the upper layers via the abandoned motherbore.

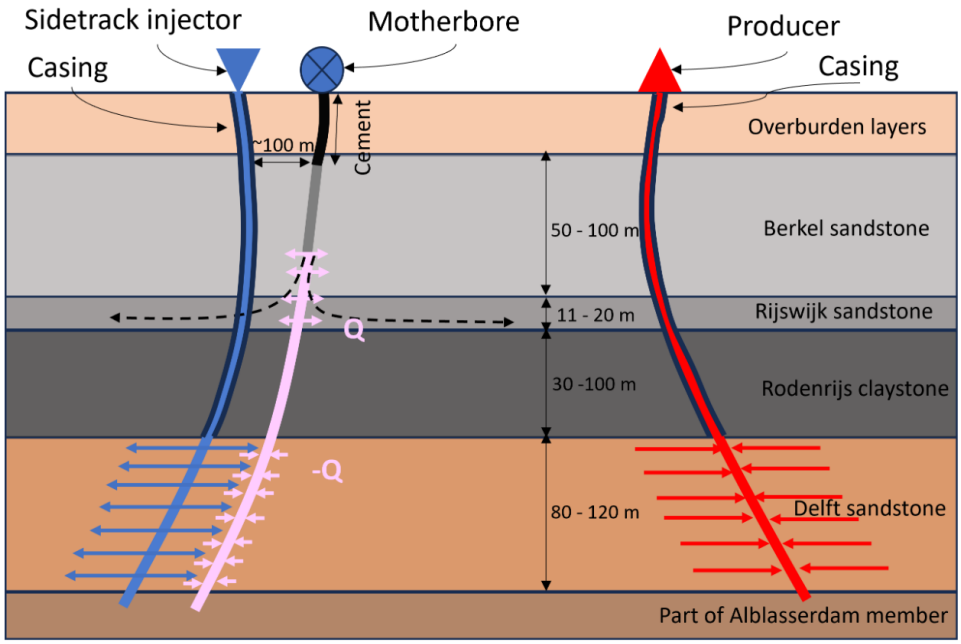

Figure 9. Schematic view of the sidetrack well, the motherbore (original injection well) and the production well. The grey section of the motherbore is assumed inactive and the pink part is assumed to be hydraulically connected to the reservoir. The dashed lines around the motherbore indicate the pressure profile along the motherbore.

Table 6. The maximum and minimum conductivity and skin factor of upper layers

	permeability × thickness (10^{-12}m^3)	skin factor (-)
Berkel sandstone, max PI parameters	129	4
Berkel sandstone, min PI parameters	32	7
Rijswijk sandstone, max PI parameters	9.9	4
Rijswijk sandstone min PI parameters	2.2	7
Rodenrijs claystone, max PI parameters	0.5	4
Rodenrijs claystone, min PI parameters	0.01	7

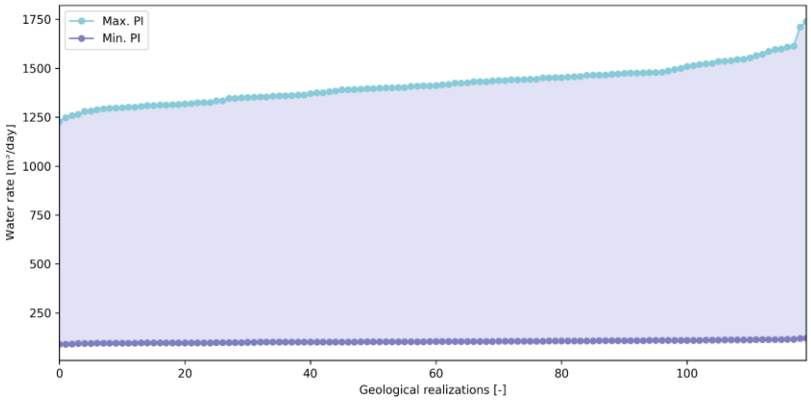

Figure 10. Steady state water rate to the upper layers

4. CONCLUSIONS

We created 120 high-fidelity geological models based on seismic interpretation, well log interpretation, facies modeling and property modeling incorporating the GTD wells' data. We investigated the effect of the abandoned motherbore on thermal production, using a worst-case sceneario of no change in shape and properties. Due to the injection operation closing to the new sidetrack injector, the cold water could flow through the motherbore to the upper permeable layers and cool down a larger column of rock than expected from injection to the reservoir only. Using the same ensemble, we evaluate the risk of water injection to the upper layers through the motherbore. Simulation results show the water loss ratio ranges from 1.5% to 20% of the original discharge rate.

In future work, we will refine the estimation of water loss to the upper layers by improving the geological understanding of the upper layers. After we obtain the temperature distribution of the top layers, we will investigate the potential risks associated with the cooling down of the larger formation volume.

5. ACKNOWLEDGEMENTS

We would like to thank Rock Flow Dynamics for the provision of the academic license to tNavigator

REFERENCES

Verma, A., and Pruess, K.: Enhancement of Steam Phase Relative Permeability Due to Phase Transformation Effects in Porous Media, Proceedings, 11th Workshop on Geothermal Reservoir Engineering, Stanford University, Stanford, CA (1986). <Reference Style>

Wang, C.T., and Horne, R.N.: Boiling Flow in a Horizontal Fracture, Geothermics, 29, (1999), 759-772. <Reference Style>

Babaei, M., & Nick, H. M. (2019). Performance of low-enthalpy geothermal systems: Interplay of spatially correlated heterogeneity and well-doublet spacings. Applied Energy, 253, 113569. https://doi.org/10.1016/j.apenergy.2019.113569

Barnhoorn, A., Vondrak, A., Laumann, S., van Esser, B., Vargas Meleza, L., Abels, H. A., & Vardon, P. J. (2024,August 29). Geothermal project on TU delft campus - DEL-GT-01 and DEL-GT-02 wireline logs. https://doi.org/10.4121/2A7B2A63-DD7B-46BC-A275-97729B3AB348.V1

Bruhn, D. F., Wolf, K., Woning, M., Dalen, E. V., Nick, H. M., & Willems, C. J. L. (2015). The Delft AardwarmteProject (DAP): Providing renewable heat for the university campus and a research base for the geothermal community. World Geotherm. Congr.

Carslaw, H. S., & Jaeger, J. C. (1959). Conduction of heat in solids (2nd). Oxford University Press.

Chen, Y., Voskov, D., & Daniilidis, A. (2025). Rigorous Numerical Methodology and Heat Recovery Analysis for Modeling of Direct Use Geothermal Systems. Geoenergy Science and Engineering, 247, 213661. https ://doi.org/10.1016/j.geoen.2025.213661

Dejtrakulwong, P., Mukerji, T., & Mavko, G. (2009). Investigating thomas-stieber model for property estimationof thin-bedded shaly-sand reservoirs. SEG Technical Program Expanded Abstracts 2009, 1965–1969. https://doi.org/10.1190/1.3255240

Donselaar, M. E., & Overeem, I. (2008). Connectivity of fluvial point-bar deposits: An example from the Miocene huesca fluvial fan, ebro basin, spain. AAPG Bulletin, 92 (9), 1109–1129. https ://doi.org/10.1306/04180807079

Gilding, D. (2010). Heterogeneity determination of the delft subsurface for heat flow modelling [Master's thesis]. TUDelft.

Holden, L., Hauge, R., Skare, Ø., & Skorstad, A. (1998). Modeling of fluvial reservoirs with object models. Mathematical Geology, 30 (5), 473–496. https://doi.org/10.1023/A:1021769526425

Liu, G., Pu, H., Zhao, Z., & Liu, Y. (2019). Coupled thermo-hydro-mechanical modeling on well pairs in heterogeneous porous geothermal reservoirs. Energy, 171, 631–653. https://doi.org/10.1016/j.energy.2019.01.022

Lund, J. W., & Toth, A. N. (2021). Direct utilization of geothermal energy 2020 worldwide review [ISBN: 0375-6505Publisher: Elsevier]. Geothermics, 90, 101915.

Major, M., Daniilidis, A., Hansen, T. M., Khait, M., & Voskov, D. (2023). Influence of process-based, stochastic and deterministic methods for representing heterogeneity in fluvial geothermal systems. Geothermics, 109.https://doi.org/10.1016/j.geothermics.2023.102651

Muskat, M. (1936). The flow of homogeneous fluids through porous media [Reprinted by J. W. Edwards, Publisher,Inc., Ann Arbor, 1937]. McGraw-Hill Book Company.

Pandey, S., Vishal, V., & Chaudhuri, A. (2018). Geothermal reservoir modeling in a coupled thermo-hydro-mechanical-chemical approach: A review. Earth-Science Reviews, 185, 1157–1169. https ://doi.org/10.1016/j.earscirev.2018.09.004

Rock Flow Dynamics. (2024). Tnavigator (Version 24.2) [Academic license provided by Rock Flow Dynamics].https://rfdyn.com

Chen et al.Stieber, S. (1970). Pulsed neutron capture log evaluation - louisiana gulf coast. Fall Meeting of the Society of Petroleum Engineers of AIME, SPE–2961–MS. https://doi.org/10.2118/2961-MS

ThermoGIS. (2023). Thermogis v2.3 (april). https://www.thermogis.nl/en/thermogis-v23-april

Tiab, D., & Donaldson, E. C. (2016). Porosity and permeability. In Petrophysics (pp. 67–186). Elsevier.

TNO. (1977). Dutch oil and gas portal. https://www.nlog.nl/

Vardon, P., Abels, H., Barnhoorn, A., Daniilidis, A., Bruhn, D., Drijkoningen, G., Elliott, K., van Esser, B., Laumann, S., van Paassen, P., Vargas Meleza, L., Vondrak, A., & Voskov, D. (2024). A Research and Production Geothermal Project on the TU Delft Campus: Project Implementation and Initial Data Collection. 49th Workshop on Geothermal Reservoir Engineering 2024, 1–7. https://pangea.stanford.edu/ERE/db/GeoConf/papers/SGW/2024/Vardon.pdf

Voskov, D., Abels, H., Barnhoorn, A., Chen, Y., Daniilidis, A., Drijkoningen, G., Geiger, S., Laumann, S., Song, G.,Vardon, P. J., Meleza, L. V., Verschuur, E., & Vondrak, A. (2024). A research and production geothermal project on the TU delft campus: Initial modeling and establishment of a digital twin. 49th Workshop on Geothermal Reservoir Engineering 2024. https://pangea.stanford.edu/ERE/db/GeoConf/papers/SGW/2024/Voskov.pdf

Voskov, D., Saifullin, I., Novikov, A., Wapperom, M., Orozco, L., Seabra, G. S., Chen, Y., Khait, M., Lyu, X.,Tian, X., De Hoop, S., & Palha, A. (2024). Open delft advanced research terra simulator(open-DARTS).Journal of Open Source Software, 9 (99), 6737. https://doi.org/10.21105/joss.06737

Willems, C. J., Vondrak, A., Mijnlieff, H. F., Donselaar, M. E., & Van Kempen, B. M. (2020). Geology of the upper jurassic to lower cretaceous geothermal aquifers in the west netherlands basin – an overview. Netherlands Journal of Geosciences, 99, e1. https://doi.org/10.1017/njg.2020.1